Polymer Nanocomposites: In Situ Polymerization of Polyamide 6 in the Presence of Graphene Oxide

Aidan O'Neill,[1] Edward Archer,[2] Alistair McIlhagger,[2] Patrick Lemoine,[1] Dorian Dixon[1]
[1]*Nanotechnology and Integrated BioEngineering Centre (NIBEC), University of Ulster, Belfast, Northern Ireland BT370QB, UK*

[2]*Northern Ireland Advanced Composite Engineering (NIACE), University of Ulster, Belfast, Northern Ireland BT370QB, UK*

Polyamide 6 (PA6)/graphene oxide (GO) nanocomposites were prepared via in situ, ring opening polymerization of ε-caprolactam in the presence of both dried powder and colloidally dispersed single layer GO. Characterization of the composites and GO (both as received and after removal from the composites) was carried out using atomic force microscopy (AFM), Fourier transform infra-red spectroscopy (FTIR), Raman spectroscopy, X-ray photoelectron spectroscopy (XPS), X-ray diffraction (XRD), thermogravimetric analysis, differential scanning calorimetry and tensile testing. Reduction in the GO during polymerization was observed. So too was functionalization of the GO flakes with PA6 chains. FTIR demonstrates the retention of some carbonyl oxygen functionalities after polymerization. AFM imaging indicated the presence of single layer GO and the sheet height increased to ~4 nm for graphene sheets after polymerization. This suggests the graphene acts as a base for polymer chain formation, leading to good interfacial interaction between the filler and matrix. Raman data show no evidence of the restoration of sp2 hybrid as a result of polymerization. The nanocomposites are thermally stable while molecular weight and crystallinity have both been affected by GO inclusion. A percentage linear increase in Young's modulus was observed as colloidally dispersed GO content increased. POLYM. COMPOS., 00:000–000, 2015. © 2015 Society of Plastics Engineers

INTRODUCTION

Graphene is a two-dimensional sheet comprised of carbon atoms arranged in a hexagonal honeycomb structure [1]. There is a concerted international research effort aimed at exploiting the material's extraordinary properties [2]. These include excellent mechanical properties with a reported Young's modulus of 1 TPa and a tensile strength of 130 GPa [3]. A thermal conductivity of 5000 watts per metre Kelvin W $(m{\cdot}k)^{-1}$ [4] and an extremely high electrical conductivity of around 6000 S cm^{-1} [5]. Chemical vapour deposition, epitaxial growth and micromechanical cleavage are just a few of the methods currently used for graphene production [6]. However, these methods can produce only a limited amount of the material. The production of graphene oxide (GO) via the chemical exfoliation of graphite, in most cases using a modified Hummer's method [7], is the most feasible technique for large scale production of the nanomaterial. Consequently, it is the use of this material which receives the most interest in the development of polymeric nanocomposites [8].

Polyamide 6 (PA6) is a thermoplastic, semicrystalline condensation polymer that is notable for its high moisture absorption [9]. Better known as Nylon 6; its wear resistance, toughness, excellent mechanical performance, and chemical resistance lead to its use in a range of applications. Including self lubricating gears, bearings, fibres, under the hood automotive applications, and use in various commodities. Nanocomposite fabrication can produce high performance and light weight materials; with uses as high strength structural materials and anti-scratch coatings for lens and surface protection. To exploit the enhanced properties of nanomaterials such as graphene in bulk materials it is essential to incorporate them into a composite material, frequently into a polymer matrix [10]. Relative to neat polymers; improvements have been observed in flammability resistance, enhanced thermal and electrical properties, and most commonly mechanical reinforcement. Use in biomedical applications and fuel cells have also been reported [11]. The evidence for previously prepared PA6/Graphene nanocomposites suggests they achieved good interfacial bonding with the polymer [12]. Improvements in thermal properties such as onset degradation temperature [13], while mechanical improvements in tensile strength and Young's moduli have also been recorded [14]. Contrasting changes in the affect on

Correspondence to: Dorian Dixon; e-mail: d.dixon@ulster.ac.uk
DOI 10.1002/pc.23612
Published online in Wiley Online Library (wileyonlinelibrary.com).

crystallinity have been reported with graphene inclusion [15, 16]. The reduction in GO during polymerization is also attested [17]. The main obstacles to achieving improvements are adequate dispersion and interfacial bonding. A range of techniques have been used to prepare graphene nanocomposites including melt mixing [18], covalent functionalization [19], addition of chemical groups such as surfactants [20], dispersion into solvents [21], and in situ polymerization. In situ polymerization offers great potential in transferring the properties of the graphene to the polymer [22] by producing composites with graphene sheets that are well dispersed throughout and attached to the host matrix.

This work focuses on the preparation and characterization of a number of PA6/GO nanocomposites via in situ ring opening polymerization of ϵ-caprolactam in the presence of both colloidally dispersed and dried powder GO, with the aim of understanding the effect of in situ polymerization on the properties of GO and its oxidative state. The properties of the nanocomposites will also be examined. The use of colloidally dispersed GO may offer some advantages over composites, which have been prepared using a dried GO powder and reduced GO, as detailed in previous work [23].

EXPERIMENTAL

Materials

Single layer GO dispersed in water was purchased from ACS Materials (10 mg ml^{-1}). GO powder was purchased from NanoInnova Technologies. ϵ-Caprolactam ($C_6H_{11}NO$, 99%), 6-amino caproic acid ($C_6H_{13}NO_2$, 99%), formic acid (CH_2O_2, 98%), and ethanol (C_2H_6O, 99.5%) were purchased from Sigma-Aldrich.

Preparation of PA6 and Composites

Thirty grams of ϵ-caprolactam was placed into a 50-ml round-bottomed flask on a temperature controlled hot plate with a magnetic stirrer, inside a fume hood and under an inert argon atmosphere. The temperature was raised to 80°C to melt the caprolactam and a magnetic flea was used to stir throughout polymerization. Colloidally dispersed GO was then added by pipette in the required amounts to give weight percentage (wt%) composites of 0.1 wt%, 0.25 wt%, 0.5 wt%, 0.75 wt%, and 1 wt%, by dropping 1 ml (10 mg ml^{-1}) at a time into the solution and allowing the water to evaporate. Dried GO powder was added in the same wt% amounts. Neat PA6 samples for controls where produced with and without water. After addition of GO at 80°C the solutions were tip sonicated for 30 min. The polymerizable mixture was then held at 150°C at which point 10 wt% of 6-amino-caproic acid (3 g) was added. The temperature was then raised as follows: 150°C for 30 min, 200°C for 30 min, 225°C for 30 min, and finally 250°C for 5 h [13, 15, 17]. The resulting viscous polymer was poured into boiling water and allowed to cool. The material was then chopped into small pieces which were washed in a beaker of boiling water for approximately 2 h. This washing was repeated four times to remove any unreacted monomer. All samples were dried overnight under vacuum at 85°C.

Characterization

Atomic force microscopy (AFM) was carried out using a VEECO DI 3100 Scanning Probe Microscope system in gentle tapping mode at a scanning frequency of 1 Hz. A TESP (n) doped silicon tip was used (stiffness approximately 40 Nm^{-1}, approximately 274–386 kHz resonance frequency).

Fourier transform infra-red spectroscopy (FTIR) was conducted using a Varian 640 IR FT-IR spectrometer over a range of 4000–400 cm^{-1} at a resolution of 4 cm^{-1} in absorbance mode. The powder samples were analyzed by diffuse reflectance infra-red Fourier transform spectroscopy (DRIFTs) using potassium bromide as a background.

Raman Spectroscopy was carried out using an ISA Labram 300 confocal Raman spectroscope with a 632.8-nm helium-neon laser and a 1-μm spot size. A charged coupled camera and backscattering geometry was used to collect spectra from 400 to 4000 cm^{-1}. Exposure times of 10 s were used along with a laser power of 10 mW.

High resolution X-ray photoelectron spectroscopy (XPS) of samples was carried out using a Kratos Axis Ultra DLD spectrometer using a monochromatic aluminium Kα X-ray source ($hv = 1486.6$ eV), operating at a pressure of approximately 8×10^{-9} torr, a voltage of 15 kV and a current of 10 mA. An electrostatic and magnetic hybrid lens mode was used with a 300 × 700 μm analysis area. Charging effects on samples were corrected by calibrating the lowest component of the spectral envelope of the C 1 s peak to 285 eV. Quantification of components was conducted using a Shirley background correction.

X-ray diffraction (XRD) data were acquired using a Bruker D8 Discover X-ray diffractometer, with a step size of 0.04°, a time per step of 60 s and voltage and current settings of 40 kV and 20 mA, respectively, using a monochromatic Cu Kα source ($\lambda = 1.5418$ Å).

Tensile testing of composites was performed using a Zwick/Roell (Ulm, Germany) ProLine, machine (5 kN load cell) under uniaxial stress with a cross head speed of 20 mm min^{-1}. Testing was carried out at room temperature using ASTM standard D638 Type V samples; the dimensions of which are 63.5 mm length, 9.53 mm gauge length, and 3.18 mm width. Thickness was measured separately for each sample at three points within the testing area. At least five specimens where tested for each sample type.

Thermogravimetric analysis (TGA) was carried out using a Mettler Toledo DSC1 STAR^e system with a 10-

 DOI 10.1002/pc

mg sample size under a flowing nitrogen atmosphere over a temperature range of 30–600°C and at a heating rate of 1°C per minute.

Differential scanning calorimetry (DSC) was conducted using a Mettler Toledo TGA/SDTA 851[e] with a 10-mg sample size in a flowing nitrogen atmosphere in the temperature range 30–600°C at a heating rate of 1°C per minute. Samples were preconditioned in the DSC at 50°C for 2 min before analysis.

Sample Preparation

Post polymerization graphene samples were obtained by dissolving approximately 1 g of composite in 50 ml of formic acid, then centrifuging the solution using a Heraeus 17RS centrifuge at 10,000 rpm for 90 min. Approximately 49 ml supernatant was then removed using a pipette to remove any free polymer, and approximately 49 ml of formic acid added to make the volume back up to 50 ml. This solution was then centrifuged again at 10,000 rpm for 90 min to obtain a pellet of functionalized graphene which was free from any unattached polymer. AFM samples were prepared by drop drying GO dispersed in water (sonicated for 2 h) at a concentration of 0.2 mg ml^{-1} onto silicon substrates then drying at 40°C. Samples for XPS, XRD, Raman, and FTIR were prepared by drop drying GO dispersed in water (sonicated for 2 h) at a concentration of 1 mg ml^{-1} onto silicon substrates and drying at 40°C. Functionalized graphene samples were dispersed in formic acid. Samples for TGA and DSC were prepared by drying the GO dispersion in an oven at 40°C overnight.

Samples for tensile testing were moulded using a Thermo Scientific HAAKE MiniJet II injection moulder with cylinder and mould temperatures of 255°C and 55°C, respectively. Cylinder and mould pressures were 300 bar and 150 bar.

Note on the display of results: the GO dispersion and GO powder have similar results for FTIR, Raman, XPS, XRD and thermal analysis. GO powder results are published in earlier work (23). In light of this, only the data for GO dispersed in water (before and after removal from composite) are shown (GO and f-GO); except in the case of AFM and Tensile testing where the results are all new. This also applies to PA6 controls produced with and without water.

Henceforth, the GO dispersed in water will be named GO. While the GO powder will be named as such. Colloidally dispersed GO after removal from composite post polymerization will be referred to as functionalized-GO (f-GO) whereas the GO powder after removal from composite will be named f-GO powder.

RESULTS AND DISCUSSION

In Fig. 1, the presence of single layer GO is confirmed by AFM imaging showing a sheet height of 0.86 nm for GO dispersed in water and 0.91 nm for GO powder [24, 25]. It is illustrated that the thickness and morphology of the GO before and after polymerization show substantial differences; with the GO sheet height increasing from 0.86 nm to approximately 4 nm postpolymerization [14]. The same is seen with GO powder samples increasing from 0.91 nm to 3.6 nm. This increase in flake height demonstrates that the in situ polymerization causes attachment of PA6 chains to the surface of GO. It is not known whether this functionalization is covalent or noncovalent [26]. Physisorption is a distinct possibility, however a possible mechanism for chemisorption is the reaction between carboxylic acid groups on the edge of GO and the amino acid end groups of PA6 chains [15]. Lateral sheet size does not seem to have been greatly affected by the polymerization or tip sonication processes with sizes ranging from hundreds of nanometres to 1-2 microns. However the largest sheet sizes of GO are not present in f-GO samples suggesting perhaps the breakup of the largest sheets by tip sonication and the subsequent polymerization. This is especially prevalent in Fig. 1C) with a sheet 2.7 μm wide, whereas for post polymerization samples no such large sheets are seen.

F-GO samples can achieve much more stable suspension in formic acid compared with GO due to grafted polymer chains on the graphene surface and their affinity for organic solvents [27]. Centrifugation should remove any free PA6 so the presence of bound PA6 on the surface of GO will promote good interfacial adhesion between the polymer and graphene, and should assist with dispersion. F-GO could not be dispersed in water giving weight to the idea of reduction during polymerization as GO is easily dispersed owing to oxygen groups promoting hydrophilicity [28].

In Fig. 2, the peaks in the FTIR spectra located at 3650 cm^{-1}, 1750 cm^{-1}, 1625 cm^{-1}, 1410 cm^{-1}, and 1225 cm^{-1} and between 1050 and 1150 cm^{-1} are attributed to the functional groups hydroxyl (C—OH), carbonyl and double bound carboxyl (C═O), aromatic carbon (C═C), single bound carboxyl (C—O), basal plane epoxide (C—O—C) and alkoxy (C—O), respectively [29, 30]. The peaks due to these oxygen functionalities are greatly reduced in f-GO spectra. This shows the lack of oxygen functionalities on the postpolymerization samples. The loss of epoxide, carboxyl, and hydroxyl groups with the peaks at 1050–1150 cm^{-1} and 1225 cm^{-1} being absent from the functionalized samples, and the peak at 1750 cm^{-1} being greatly reduced give evidence to attest the reduction in GO. From the spectra of f-GO, it can be seen that the carbonyl functionalities represented by the discreet peak at 1750 cm^{-1} seem to be more resistant to this reduction [31].

Referring to Fig. 3, in the Raman spectra of GO the typical G peak is located at 1590 cm^{-1}. The D peak is located at 1330 cm^{-1} [32]. Subtly located at 2650 cm^{-1} is the 2D peak. While the D+D' peak is seen at 2900 cm^{-1} [33]. I_D/I_G ratio for GO is 1.15 and for f-GO it is 1.21.

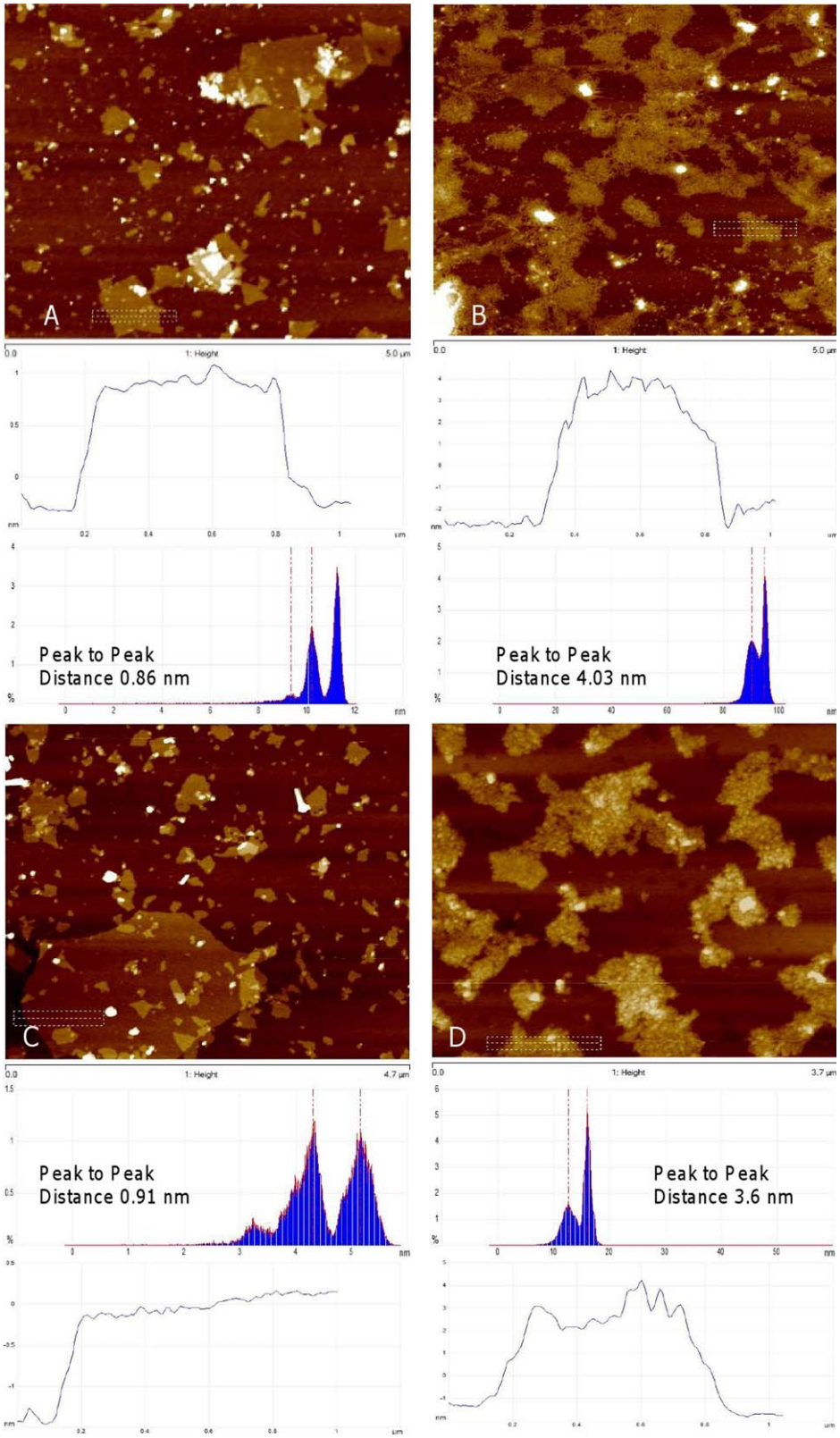

FIG. 1. Pseudo-colored AFM images including depth and step profiles of pre- and postpolymerization GO. (A) GO flakes with a height of approximately 0.8 nm and (B) f-GO flakes with a height of approximately 4 nm. (C) GO powder with a height of approximately 0.9 nm and (D) f-GO powder with a height of 3.6 nm. The depth profile is taken of the whole image, whereas step height is taken from the region shown by the dotted white line. [Color figure can be viewed in the online issue, which is available at wileyonlinelibrary.com.]

 DOI 10.1002/pc

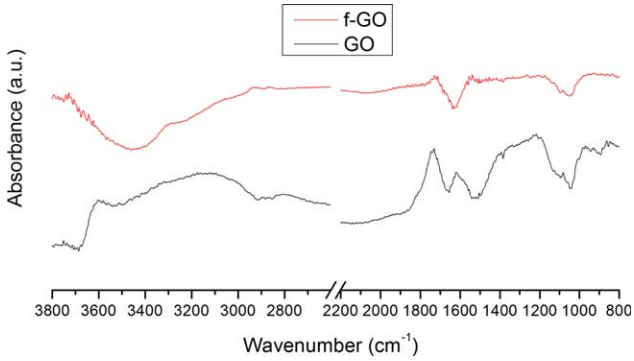

FIG. 2. FTIR absorbance spectra showing GO (bottom) and f-GO (top). [Color figure can be viewed in the online issue, which is available at wileyonlinelibrary.com.]

Raman spectroscopy is extensively used to study disorder and defects in nanostructured carbon materials [34]. The absence of a sharp 2D peak is due to the presence of functional groups such as epoxide and hydroxyl which transforms the carbon atoms from planar sp^2 hybridized to distorted sp^3 hybridized orbitals. The lack of a significant change in the I_D/I_G ratio would suggest that the reduction in GO has not restored the sp2 hybrid for post polymerization GO. It is assumed that although the oxygen has been removed the sp2 network has not been restored and defects are still present. The 2D peak at 2650 cm^{-1} indicates the presence of single layer GO [33], as this peak arises due to intact sp2 regions [35]. This supports the AFM results by further demonstrating monolayer GO. It is assumed that while there are clusters of sp2 hybridized atoms present, the low intensity and high FWHM of the peak suggest these are sparsely located, possibly situated in small regions between oxygen functionalities.

Wide energy XPS survey scans for GO, f-GO, and PA6 are shown in Fig. 4: A which displays peaks at approximately 285 eV, 400 eV, and 532 eV, which are attributed to C 1s, N 1s, and O 1s, respectively. GO C 1s components were peak fitted to four spectral components: C—C at 285 eV, C—O at 287.1 eV, C═O at 287.9 eV, and O═C—OH at 288.9 eV. PA6 C 1s peak was fitted to

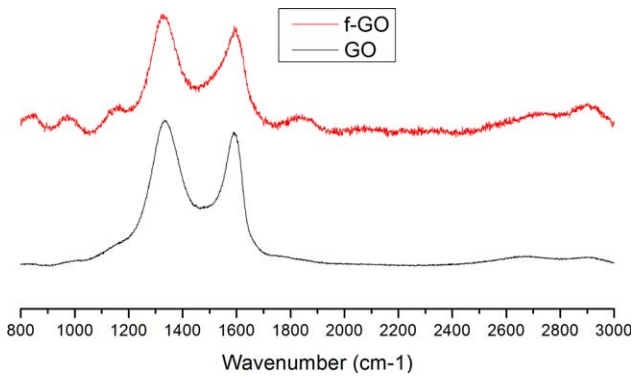

FIG. 3. Raman spectra of GO (bottom) and f-GO (top). [Color figure can be viewed in the online issue, which is available at wileyonlinelibrary.com.]

the following components: C—C at 285 eV, C—C═O at 285.8 eV, C—N at 286.2 eV, and CONH at 288 eV. The f-GO C1s peaks were located as follows: C—C at 285 eV, C—C═O at 285.7 eV, C—N at 286.2 eV, and CONH at 288 eV [36, 37].

XPS data coincide with the Lerf-Klinowski and Dékány models for GO with epoxide and hydroxyl groups present on the basal plane with carboxyl and carbonyl (ketone) edge groups [38, 39]. As outlined in our previous work this XPS further supports the reduction in GO during polymerization, with a lack of the prominent C—O peak at approximately 287 eV in f-GO. The dominance of PA6 peaks in post polymerization GO samples supports the idea of the functionalization of graphene flakes via polymer chain propagation from the surface. The C—O peak in GO occurs at the same binding energy as C—C═O for PA6 samples (approximately 285.8 eV). The C—O peak is a mixture of C—OH (hydroxyl) and C—O—C (epoxide) bonds with hydroxyl occurring at a lower binding energy [36]. Upon reduction, the C—O peak eV appears to lower to 285.8 eV when in fact this is due to hydroxyl groups making up the majority of oxygen functional groups present. With higher binding energy epoxy groups having been removed during polymerization which takes place at temperatures up to 250°C.

Figure 5 shows that the X-ray diffraction pattern for GO gives a sharp peak at $2\theta = 10.7°$, which is brought about by intercalated water molecules and oxygen functionalities and corresponds to an interlayer spacing of 0.83 nm (002). Peaks in the diffraction pattern for f-GO are observed at 20.3° and 24.2° and coincide to previously reported peaks for reduced GO (rGO) and correspond to interlayer spacings of 0.44 nm and 0.37 nm, respectively. These are attributed to spacings between the carbon layers depending on the amount of graphitization or oxidation [40]. All additional peaks observed in samples above 25° are attributed to either graphite, graphite oxide or exfoliated graphite including the distinct peak at 54° (004) in f-GO samples [41]. In 5: B, there are three peaks present. The peak at 21.2° is assigned to γ phase crystallites in PA6. Peak locations at 20.5° and 23.2° are attributed to α phase crystallites [42].

Pristine single layer graphene does not have an interlayer spacing thus the presence of any peaks in the XRD patterns indicates that along with single layer GO there is also some multilayer material present. Values in the literature for the d-spacing of GO vary from around 0.65 nm [43] to 0.96 nm [44] depending on the degree of exfoliation and various oxide groups present. The d-spacing of 0.83 nm in our GO samples is attributed to the amount of interlamellar water present between the hydrophilic sheets [45]. Reduction in the GO during polymerization is further established owing to the fact that the data for f-GO replicates the diffraction pattern for rGO with d-spacing's of 0.37 and 0.43 nm [43], while having no sign of the GO identifying peak at 10.7° [46]. It could be assumed that along with reduction there has also been a little

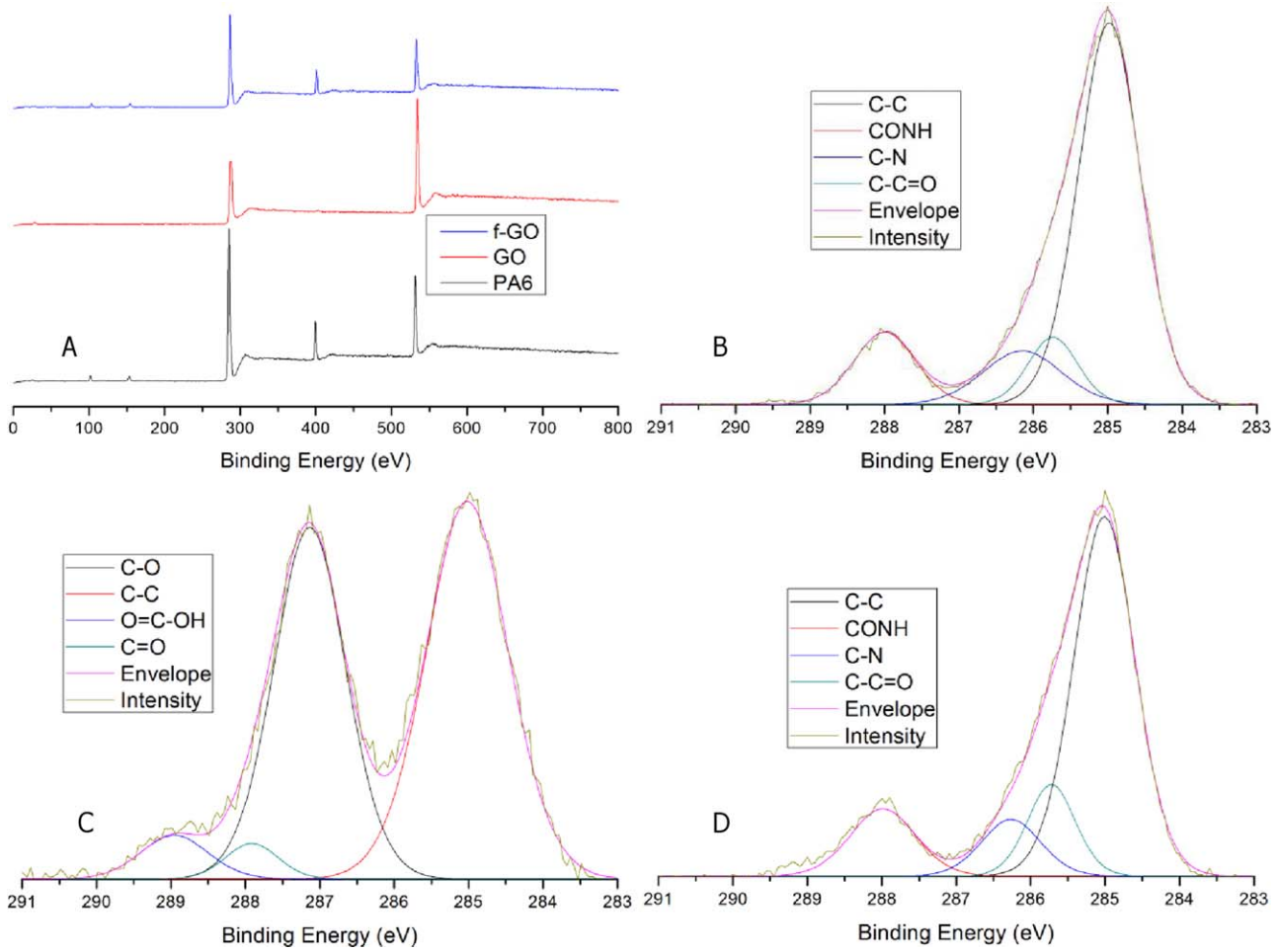

FIG. 4. Shows (A) XPS wide energy survey scan for GO, f-GO, and PA6; (B) peak fitted C1s for PA6; (C) Peak fitted C 1s for GO; (D) Peak fitted C 1s for f-GO. [Color figure can be viewed in the online issue, which is available at wileyonlinelibrary.com.]

restacking of GO sheets after polymerization due to the presence of a graphitic peak at 54° [47]. However, the functional groups present in GO should dissociate interactions in the carbon backbones between sheets thus keeping them apart [36]. So rather than the single layer sheets restacking; it is quite possible that the same partially

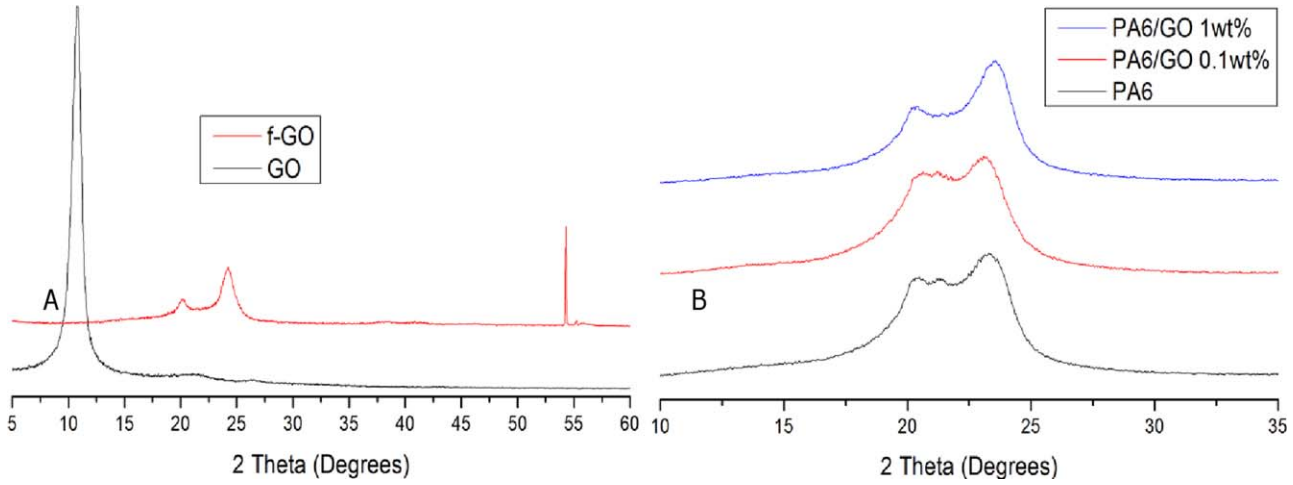

FIG. 5. XRD pattern of (A) GO and f-GO and (B) in ascending order PA6, PA6/GO 0.1wt% and PA6/GO 1wt%. [Color figure can be viewed in the online issue, which is available at wileyonlinelibrary.com.]

DOI 10.1002/pc

TABLE 1. Ultimate tensile strength (UTS), yield strength (YS), Young's modulus (E), and percentage elongation at break for PA6 (made with water) and PA6/GO composites.

Sample	UTS (MPa)	YS (MPa)	E (MPa)	Elongation at break (%)
PA6	60.4	45.9	469.4	479
PA6/GO 0.1 wt%	58.2	49.7	522.8	327
PA6/GO 0.25 wt%	61.2	48.8	553.5	388
PA6/GO 0.5 wt%	52.5	52	571.3	372
PA6/GO 0.75 wt%	62	51.2	597	201
PA6/GO 1 wt%	53.4	53.3	600	177

exfoliated layers that are detected in the pattern for GO, after having the intercalated water molecules and oxygen groups removed from between them, then make up the peaks for rGO and graphite that are seen in f-GO samples. Both α and γ phase crystallites are present in the neat PA6. This is caused by the cooling of PA6 and nanocomposites during preparation [42]. It is quite clear that for PA6/GO 1 wt% there is no prominent γ phase peak thus leading to the conclusion that GO inclusion has either inhibited the formation of the γ phase or promoted the growth of α phase crystallites. The α phase typically occurs in quenched PA6 while a mixture of α and γ phases is seen in annealed samples [48].

The mechanical properties of the control PA6 are in general agreement with values in the literature which vary greatly due to the polymer processing techniques and differences in percentage crystallinity [13, 49]. When compared with the properties of control PA6 made using water (Table 1, 469.4 MPa) the control PA6 produced without water has an average Young's modulus of 612 MPa. This shows that the use of water has a detrimental affect on the mechanical properties of PA6. Immediate improvements are seen in Young's modulus and yield strength with even the lowest colloidally dispersed GO content. While elongation at break decreases. This is attributed to the GO interrupting the growth of polymer chains causing a lower molecular weight [14].

Tensile results (Fig. 6) for dried GO powder composites have no linearity and in all cases have decreased Young's modulus when compared with neat PA6. Results for PA6/GO composites show a linear increase in Young's modulus as graphene content increased from 0.1 wt% to 1 wt% with a total of a 28% increase for PA6/GO 1 wt%. Elongation at break shows a linear decrease with increased filler content as the material becomes stiffer and less flexible [50]. Improvement in yield strength seems apparent of not substantial. For PA6/GO 1 wt% yield strength has improved by 16%, however, results are not linear with increasing wt%. Compared with GO powder the results for GO dispersion nanocomposites are substantially better, suggesting that the use of GO dispersed in water yields better dispersion and, therefore, better mechanical performance. However, the use of water weakens the materials properties overall and makes it difficult to add a high wt% of filler as the mixture has already begun polymerization by the time the last of the dispersion is added.

Referring to Fig. 7, the weight loss curve for GO shows an initial 10% moisture loss at approximately 100°C, proceded by a 30% loss at approximately 200°C as a result of oxygen loss [51]. This step is not visible in f-GO. For f-GO, sample weight loss occurs in line with that of PA6 with an onset degradation temperature of 369°C, due to the large amount of polymer attached to the now reduced GO sheets. PA6 and composites samples undergo degradation between 350 and 425°C [52]. Further decomposition occurs up to 600°C for all samples.

The 30% mass loss is indicative of the reduction in GO [28]. The introduction of graphene into the polymer

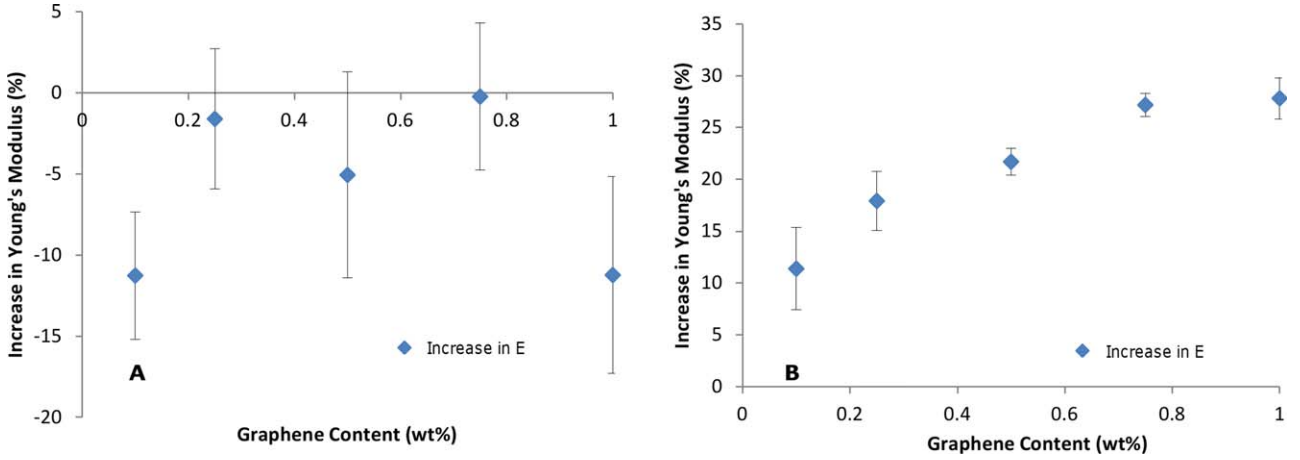

FIG. 6. Average percentage change in Young's modulus for composites with increasing GO wt% for (A) GO powder and (B) Colloidally dispersed GO. (A) has as a baseline representative of the mechanical properties of PA6 produced without water. While (B) reports a baseline of PA6 produced with water. [Color figure can be viewed in the online issue, which is available at wileyonlinelibrary.com.]

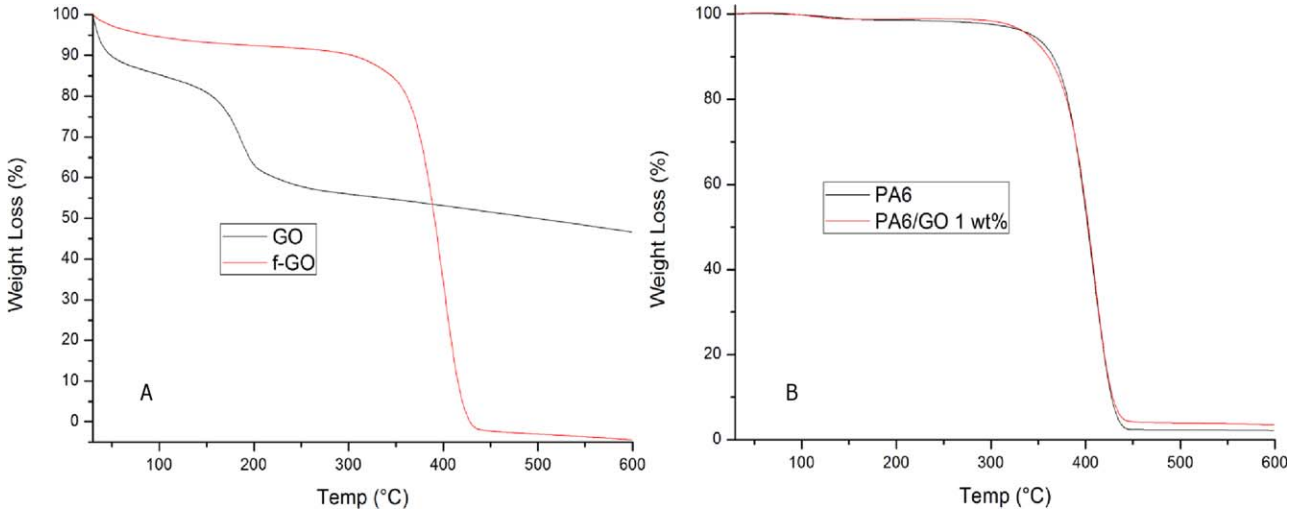

FIG. 7. TGA weight loss curves for (A) GO and f-GO and (B) neat PA6 and PA6/GO 1 wt%. [Color figure can be viewed in the online issue, which is available at wileyonlinelibrary.com.]

matrix has had no detrimental effects on the properties of the polymer as the composites are thermally stable up to approximately 350°C. Reduction in the GO during polymerization is attested by the absence of the 30% weight loss step at 200°C in the post polymerization samples, as the oxygen has by now been thermally decomposed during polymerization [17] or degraded into conjugated bonds [15]. The onset degradation of PA6/GO 1 wt% is 378°C compared with 372°C for PA6. While a 6°C change is only a modest increase in degradation temperature; several previous papers have attributed this to char formation caused by the filler material, which degrades at higher temperatures and slows degradation by shielding the polymer [53, 54].

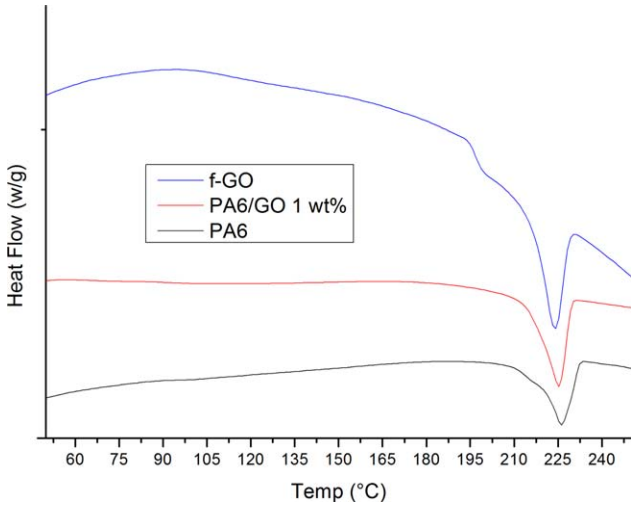

FIG. 8. DSC exothermic curve for neat PA6, PA6/GO 1 wt%, and f-GO. [Color figure can be viewed in the online issue, which is available at wileyonlinelibrary.com.]

DSC data in Fig. 8 reveal that for control PA6, PA6/GO 1 wt% and f-GO an exothermic peak is observed between 210°C and 230°C. With peak locations at 226.5°C, 224°C, and 220.5°C, respectively. This peak corresponds to the melting point of the material [42] specifically the melting of γ phase crystals. While the smaller melt peak before 210°C is due to the melting of α phase crystals [55] (Table 2).

The lower melting temperature in PA6/GO 1 wt% and f-GO when compared with that of neat PA6 is thought to be due to the graphene inhibiting polymer chain propagation resulting in a lower molecular weight, especially for the polymer bound to the graphene surface [56]. Melt enthalpy (ΔH_m) is increased from 60.6 J g^{-1} for control PA6 to 74.7 J g^{-1} for PA6/GO 1 wt%. This is because graphene acts as a nucleation point for crystallites [13]. An increase in ΔH_m for composites indicates an increase in the percentage crystallinity of nanocomposite PA6 [16, 52]. A further increase to 83.9 J g^{-1} for f-GO samples indicates that percentage crystallinity is increased further for PA6 that is directly attached to the graphene.

TABLE 2. Onset degradation temperatures, residual material, melting points, and melt enthalpy from TGA and DSC analysis.

Method	TGA		DSC	
Sample	Onset degradation (°C)	Residual material (%)	Melting temperature (°C)	Melt Enthalpy ΔH_m (J g^{-1})
PA6	372	2.1	226.5	60.6
PA6/GO 1 wt%	378	3.5	225.2	74.7
GO	168	46.6	–	–
f-GO	369	3.6	224	83.9

DOI 10.1002/pc

CONCLUSION

In this work the in situ preparation and characterization of a number of PA6/GO composites are reported, with a focus on the properties of the GO before and after polymerization. After polymerization, functionalization of graphene sheets with PA6 is observed along with reduction in the oxygen species. This reduction is thought to be mainly thermal however some oxygen may be lost in bonding with the polymer. A small quantity of doubly bound oxygen is shown to be retained by FTIR in the post polymerization samples. The use of colloidally dispersed GO obtains much better mechanical improvements compared with the use of dried GO powder. Interfacial interaction seems to be excellent in the composites due to the amount of functionalization on f-GO sheets and the improvement in Young's modulus at low GO content. It would seem that wetting is adequate for both GO powder and colloidally dispersed GO, with the colloid achieving much better dispersion. This work reports a simple method for the production of multi functional nanocomposites which could easily be produced on a large scale.

ACKNOWLEDGMENT

The authors thank NIBEC and NIACE for permitting to use their facilities and equipment and David Bishop of NIBEC for the processing of XPS samples for analysis.

REFERENCES

1. H. Kim, A.A. Abdala, and C.W. Macosko, *Macromolecules*, **43**(16), 6515 (2010).
2. R. Van Noorden, *Nature*, **469**, 14 (2011).
3. C. Lee, X. Wei, J.W. Kysar, and J. Hone, *Science*, **321**(5887), 385 (2008).
4. A.A. Balandin, S. Gosh, W. Bao, I. Calizo, D. Teweldebrhan, F. Miao, and C.N. Lau, *Nano. Lett*., **8**(3), 902 (2008).
5. K.S. Novoselov, A.K. Geim, S.V. Morozov, D. Jiang, M.I. Katsnelson, I.V. Grigorieva, S.V. Dubonos, and A.A. Firsov, *Nature*, **438**, 197 (2005).
6. K.S. Novoselov, A.K. Geim, S.V. Morozov, D. Jiang, Y. Zhang, and S.V. Dubonos, *Science* **306**(5696), 666 (2004).
7. W.S. Hummers and R.E. Offeman, *J. Am. Chem. Soc*., **80**(6), 1339 (1958).
8. S. Park and R.S. Ruoff, *Nat. Nanotechnol*., **4**, 217 (2009).
9. S.C. Tjong and S.P. Bao, *J. Polym. Sci. Part B Polym. Phys*., **42**(15), 2878 (2004).
10. W.E. Gacitua, A.A. Ballerini, and J. Zhang, *Maderas. Ciencia y tecnologia* **7**(3), 159 (2005).
11. D.R. Paul and L.M. Roberson, *Polymer*, **49**, 3187 (2008).
12. S. Das, A.S. Wajid, J.L. Shelburne, Y.C. Liao, and M.J. Green, *Appl. Mater. Interf*., **3**(6), 1844 (2011).
13. D. Dixon, P. Lemonine, J. Hamilton, G. Lubarsky, and E. Archer, *J. Thermoplast. Compos. Mater* **28**, 372 (2013).
14. X. Zhang, X. Fan, H. Li, and C. Yan, *J. Mater. Chem*., **22**, 24081 (2012).
15. Z. Xu and C. Gao, *Macromolecules*., **43**(16), 6716 (2010).
16. F. Zhang, X. Peng, W. Yan, Z. Peng, and Y. Shen, *Polym. Phys.* **49**(19), 1381 (2011).
17. D. Zheng, G. Tang, H.B. Zhang, Z.Z. Yu, F. Yavari, N. Koratkar, S.H. Lim, and M.W. Lee, *Compos. Sci. Technol*., **72**(2), 284 (2011).
18. J.W. Cho and D.R. Paul, *Polymer*., **42**(3), 1083 (2001).
19. M. Fang, K. Wang, H. Lu, Y. Yang, and S. Nutt, *J. Mater. Chem*., **19**(38), 7098 (2009).
20. M. Han, J. Yun, H. Kim, and Y. Lee, *J. Ind. Eng. Chem*., **18**(2), 752 (2012).
21. U. Khan, P. May, A. O'Neill, and J.N. Coleman, *Carbon* **48**(14), 4035 (2010).
22. M. Fermeglia, M. Ferrone, and S. Pricl, *Fluid Phase Equilib*., **212**(1–2), 315 (2003).
23. A. O'Neill, D. Bakirtzis, and D. Dixon, *Eur. Polym. J*., **59**, 353 (2014).
24. C. Botas, P. Álvarez, C. Blanco, R. Santamaría, M. Granda, and P. Ares, *Carbon*., **50**(1), 275 (2012).
25. S. Stankovich, D.A. Dikin, R.D. Piner, K.A. Kohlhaas, A. Kleinhammes, Y. Jia, Y. Wu, S.T. Nguyen, and R.S. Ruoff, *Carbon*., **45**, 1558 (2007).
26. V. Georgakilas, M. Otyepka, A.B. Bourlinos, V. Chandra, N. Kim, and K.C. Kemp, *Chem. Rev*., **112**(11), 6156 (2012).
27. S.H. Lee, D.R. Dreyer, J. An, A. Velamakanni, R.D. Piner, and S. Park, *Macromol. Rapid Comm*., **31**(3), 281 (2009).
28. D.R. Dreyer, S. Park, C.W. Bielawski, and R.S. Ruoff, *Chem. Soc. Rev*. **39**, 228 (2009).
29. R.J. Seresht, M. Jahanshahi, A.M. Rashidi, and A.A. Ghoreyshi, *Iranica J. Energy Environ*., **4**(1), 53 (2013).
30. Rattana, S. Chaiyakun, N. Witit-anun, N. Nuntawong, and P. Chindaudom, S. Oaew, *Procedia. Eng*., **32**(0), 759 (2012).
31. A. Bagri, C. Mattevia, M. Acik, Y.J. Chabal, M. Chhowalla, and V.B. Shenoy, *Nat. Chem*., **2**, 581 (2010).
32. A.C. Ferrari, J.C. Meyer, V. Scardaci, C. Casiraghi, M. Lazzeri, and F. Mauri, *Phys. Rev. Lett*., **97**(18), 187401 (2006).
33. A.C. Ferrari and D.M. Basko, *Nat. Nanotechnol*., **8**, 235 (2013).
34. P.H. Tan, W.P. Han, W.J. Zhao, Z.H. Wu, K. Chang, and H. Wang, *Nat. Mater*., **11**(4), 294 (2012).
35. R.S. Kajen, N. Chandrasekhar, K.L Pey, C. Vijila, M. Jaiswal, and S. Saravananl, *ECS Solid State Lett*. **2**(2), M17 (2013).
36. A. Ganguly, S. Sharma, P. Papakonstantinou, and J. Hamilton, *J. Phys. Chem*. **115**, 170099 (2011).
37. G. Beamson and D. Briggs, High Resolution XPS of Organic Polymers, Scienta ESCA300 Database, Wiley, Chichester (1992).
38. A. Lerf, H. He, M. Forster, and J. Klinowski, *J. Phys. Chem*., **102**, 4477 (1998).
39. T. Szabo, O. Berkesi, P. Forgo, K. Josepovits, Y. Sanakis, and D. Petridis, *Chem. Mater*., **18**, 2740 (2006).
40. I.K. Moon, J. Lee, R.S. Ruoff, and H. Lee, *Nat. Commun*., **1**, 73 (2010).
41. M.D. Levi, E.A. Levi, and D. Aurbach, *J. Electroanal. Chem*., **421**(1–2), 89 (1997).

42. S. Xie, S. Zhang, F. Wang, M. Yang, R. Séguéla, and J. Lefebvre, *Compos. Sci. Technol.* **67**(11–12), 2334 (2007).
43. H.C. Schniepp, J.L. Li, M.J. McAllister, H. Sai, M. Herrara-Alonso, D.H. Adamson, R.K. Prud'homme, R. Car, D.A. Saville, and I.A. Aksay, *J. Phys. Chem.*, **110**(17), 8535 (2006).
44. S. Bykkam, V.K. Rao, S.C.H. Chakra, and T. Thunugunta, *Int. J. Adv. Biotechnol. Res.*, **4**(1), 142 (2013).
45. V.H. Pham, H.D. Pham, T.T. Dang, S.H. Hur, E.J. Kim, and S.B. Kong, *J. Mater. Chem.*, **22**(21), 105306 (2012).
46. S. Srivastava, K. Jain, V.N. Singh, S. Singh, N. Vijayan, and N. Dilawar, *Nanotechnology*, **23**(20), 205501 (2012).
47. G. Sun, X. Li, Y. Qu, X. Wang, H. Yan, and Y. Zhang, *Mater. Lett.*, **62**, 703 (2008).
48. D. Dixon and A. Boyd, *Polymer Eng. Sci.*, **51**(11), 2203 (2011).
49. A. Peters, C.V. Alsenoy, F. Bartha, F. Bogar, M.L. Zhang, and V.V. Doren, *Int. J. Quantum Chem.*, **91**, 32 (2002).
50. O. Koysuren, S. Yesil, and G. Bayram, *J. Appl. Polym. Sci.*, **102**, 2520 (2006).
51. Y. Qian, A. Vu, W. Smyrl, and A. Stein, *J. Electrochem. Soc.*, **159**(8), A1135 (2012).
52. S. Pashaei, Siddaramaiah, M.M. Avval, and A.A. Syed, *CI&CEQ.*, **17**(2), 141 (2011).
53. K. Scully and R. Bissessur, *Thermochim. Acta.*, **490**(1–2), 32 (2009).
54. B.J. Liang, Y. Huang, L. Zhang, Y. Wang, and Y. Ma, *Adv. Funct. Matr.*, **19**(14), 2297 (2009)
55. H.E. Miltner, G.V. Assche, A. Pozsgay, B. Pukánszky, and B.V. Mele, *Polymer*, **47**(3), 826 (2006).
56. F. Wu, Y. Lu, G. Shao, F. Zeng, and Q. Wu, *Polym. Int.*, **61**(9), 1394 (2012).

 DOI 10.1002/pc